Optimisation of slanted septum core and multiple folded cavity acoustic liners for aero-engines

Suresh Palani*, Paul Murray† and Alan McAlpine‡
Institute of Sound and Vibration Research, University of Southampton, Southampton, SO17 1BJ, United Kingdom

Christoph Richter§
Rolls-Royce Deutschland Ltd & Co KG, Dahlewitz, Eschenweg 11, 15827 Blankenfelde-Mahlow, Germany

Post-print copy of conference paper presented at the AIAA Aviation Forum, Virtual Event, 2–6 August 2021

This paper reports an assessment of the performance of two novel broadband liners for aero-engine applications, under both high sound pressure level and grazing flow. Duct insertion loss predictions are made for the novel liners for downstream sound propagation, with the results compared with that of optimised conventional Single Degree-of-Freedom (SDOF) perforate liners. The novel liner configurations include a slanted porous septum concept with varying open area, and a MultiFOCAL (Multiple FOlded CAvity Liner) concept. A numerical model of the flow duct test facility is developed using the commercial finite element code, COMSOL Multiphysics. This model is used to predict the liner insertion loss in the flow duct test facility. A multi-modal sound source is used, employing the assumption of uncorrelated modes with equal energy per mode. For downstream sound propagation, a simple convected wave equation model with the standard Ingard–Myers boundary condition is shown to be sufficient to predict the liner attenuation accurately. For upstream sound propagation, predictions and measurements for a SDOF linear liner highlight the need to account for boundary-layer refraction in the numerical modelling. The refraction effect due to the mean flow boundary layer will be modelled in a follow-up paper.

I. Introduction

In future aero-engines, even with the most advanced technologies for noise reduction at source, there will be a continuing demand for passive noise reduction by acoustic liners. In addition, more effective novel acoustic liners are required to achieve the aim of noise reduction over a broad range of frequencies, particularly as future high bypass ratio engines are expected to produce lower frequency fan tones, accompanied by significant broadband noise at higher frequencies. The advanced engine nacelles also have lower lined length to diameter aspect ratio, thus reducing liner performance.

More recently, greater attention has been devoted to the design of complex liner geometries to attain improvements in aero-engine noise reduction at lower frequencies. For example, Sugimoto et al. [1] investigated the design and performance of folded cavity liners for turbofan engine inlets. Schiller and Jones [2] developed a broadband liner design concept called a variable depth liner, composed of groups of resonators tuned for different frequencies. Such complex designs appear to be an inevitable step in the evolution of acoustic liners for larger aero-engines, due to the wide range of source frequencies to be attenuated. When developing such highly effective novel liners, one has to consider not only the effect of liner parameters such as the resistive sheets, cavity geometry, cell depths, and incident sound pressure level, but also the mean flow and boundary layer effects.

*PhD Candidate, Institute of Sound and Vibration Research (ISVR), S.Palani@soton.ac.uk.
†Principal Research Fellow, Institute of Sound and Vibration Research (ISVR), pm2@isvr.soton.ac.uk.
‡Associate Professor, Institute of Sound and Vibration Research (ISVR), A.McAlpine@soton.ac.uk.
§Global Capability Owner – Noise Technology, Specialist Acoustics, RRD System Design-Noise, Rolls-Royce Deutschland Ltd & Co KG.

The final version was published in the proceedings of the conference as paper No. 2021-2172. https://doi.org/10.2514/6.2021-2172

The mean flow boundary layer over the facing sheet of liners has been shown to have a substantial effect on upstream propagation and absorption of sound in ducts [3, 4]. The velocity gradient in the boundary layer region can refract the sound field either towards or away from the liner surface depending on its propagation direction with respect to the mean flow. In order to model the sound propagation above the liner in the presence of mean flow, Myers [5] extended the work of Ingard [6] and developed a boundary condition with the assumption of an infinitely thin boundary layer region (known as a vortex sheet). This boundary condition has been demonstrated to create instabilities if not properly damped in time domain simulations when solving the Linearized Euler (LE) equations. Recently, several studies have replaced the Myers condition with more stable and improved models. For example, Rienstra and Darau [7] and Brambley [8] separately proposed modified Myers conditions. They both included a small but finite boundary layer above the impedance surface, which removes the instability while still allowing a slipping flow above the boundary layer. However, these instabilities have not been identified with the traditional liners integrated into an actual engine nacelle [9]. Gabard [10] assessed the influence of boundary layer refraction on the liner attenuation rate by solving the eigenvalue problems for uniform flow with both the Myers [5] and a modified Myers condition [8] with a fixed boundary layer thickness representative of nacelle conditions. Gabard [10] concluded that the boundary layer refraction effects cannot be ignored for upstream sound propagation. Furthermore, the accuracy of the liner attenuation rate improved when using the modified Myers condition, with Gabard recommending the use of displacement thickness to characterise the boundary layer effects. Watson and Jones [9] investigated the suitability of the Ingard–Myers and modified Ingard–Myers boundary conditions proposed by Renou and Aurégan [11], for impedance eduction with grazing mean flow for Mach numbers $M = 0.3$ and 0.5, for both upstream and downstream sound sources. The results of this study highlighted the discrepancies in the educed impedance spectra for upstream and downstream source conditions at M = 0.5. Watson and Jones concluded that the modified Ingard–Myers impedance condition improved the accuracy of the impedance eduction model.

In this paper, the main focus is on downstream propagation, where refraction effects may be neglected, as the primary objective of the current work is to perform a detailed evaluation of two novel liner concepts, called Slanted Septum Core (SSC) and MULTIple FOlded CAvity Liner (MultiFOCAL). This is achieved by using numerical modelling to predict the liner insertion loss in a flow duct test facility. First, the acoustic properties of the novel liner concepts are predicted, without grazing flow, from a normal incidence impedance test set-up numerical model for high sound pressure level (SPL) pure tone excitations. Second, normal incidence acoustic impedance measurements were made to validate the preliminary pure tone predictions, and to evaluate the fundamental no flow characteristics of the SSC and MultiFOCAL configurations at high SPLs. Then, the impedance predictions, with mean flow corrections, are used to define the lined boundary condition in the grazing flow prediction model. Ultimately, the novel liners will be manufactured and tested in the flow duct facility at the Netherlands Aerospace Centre (Royal NLR). Consequently all of the simulations in this paper are based on a grazing flow test set-up that is representative of the NLR flow duct test facility. For validation, the insertion loss of a Single-Degree-of-Freedom (SDOF) liner, with a linear layer facing sheet, is predicted for downstream and upstream multi-modal sound propagation. The predictions are for zero flow and $M = 0.3$ and 0.5, and for frequencies in the range of 100 to 6000 Hz, with a frequency step of 100 Hz.

II. Computational model

The NLR flow duct geometry is defined in Ref. [12]. The duct height is 0.3 m and the lined section length is 0.85 m. A two-dimensional axisymmetric annular duct model with 2 m inner (R_i) and 2.3 m outer radius (R_o) is used to represent the longitudinal cross section of the NLR flow duct test facility. An annular duct is adopted in order to facilitate the efficient insertion of the input modes (spinning modes with zero azimuthal order) within the COMSOL finite element (FE) code. In the limit of large hub-to-tip ratio, the annular duct approximates to a rectangular duct two-dimensional test set-up. The schematic of the annular duct model used in this study is shown in **Fig. 1**. The duct axis is x and the radial coordinate is r. The model includes unlined (hard-wall) sections of length 1 m either side of a lined section of length 0.85 m. The ratio of the length of the lined section to the duct height is approximately 2.8 which is a good representation of a nacelle bypass duct with positive flow Mach numbers [12]. For this paper, the annular duct is assumed to contain uniform mean flow, and the mean flow Mach number is set to vary from 0.0 to 0.5.

The linearised potential flow model in COMSOL is used to describe the propagation of the sound field within the duct. The same equation is solved on the boundary, at $x = 0$, on which the broadband noise source is defined. The broadband noise source can be modelled at a given frequency by assuming excitation of all the cut-on hard-wall radial duct modes with azinuthal order $m = 0$ [13, 14]. The propagating radial modes are assumed to be uncorrelated, such that the in-duct sound power transmission loss of each mode can be calculated separately, with equal energy per mode

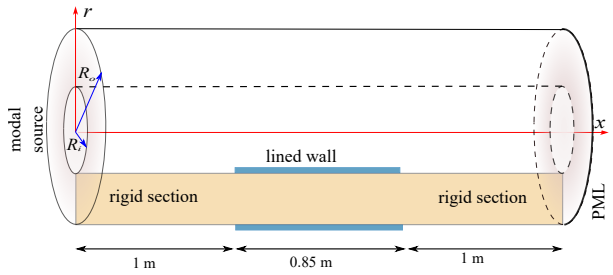

Fig. 1 Schematic of the annular duct model for liner acoustic performance assessment.

at the source plane. The power loss for different propagating modes at the same excitation frequency can be summed, because of the orthogonality of the mode shape functions, to estimate the total power loss [15]. The acoustic power of the incident radial modes is set to unity using the intensity formulation given by Morfey [16]. A reflection-free boundary condition is defined at the exit plane of the unlined termination section by using a perfectly matched layer (PML) [17]. In the lined section, the wall impedance is modelled using the Ingard–Myers boundary condition [5]. Both the inner and outer walls are lined.

III. Broadband novel liners

Fig. 2 shows the geometries of two novel liner configurations designed for broadband sound attenuation: configuration 1 – Slanted Septum Core (SSC) with two different percentage open areas; and configuration 2 – Multiple FOlded CAvity Liner (MultiFOCAL). The baseline for the geometry of the SSC and the MultiFOCAL are from the liner concepts previously patented by Murray [18], Pool et al. [19] and Murray and Astley [20], respectively, which have been developed further in this work. The complex cavities of the novel liner concepts have been designed and investigated

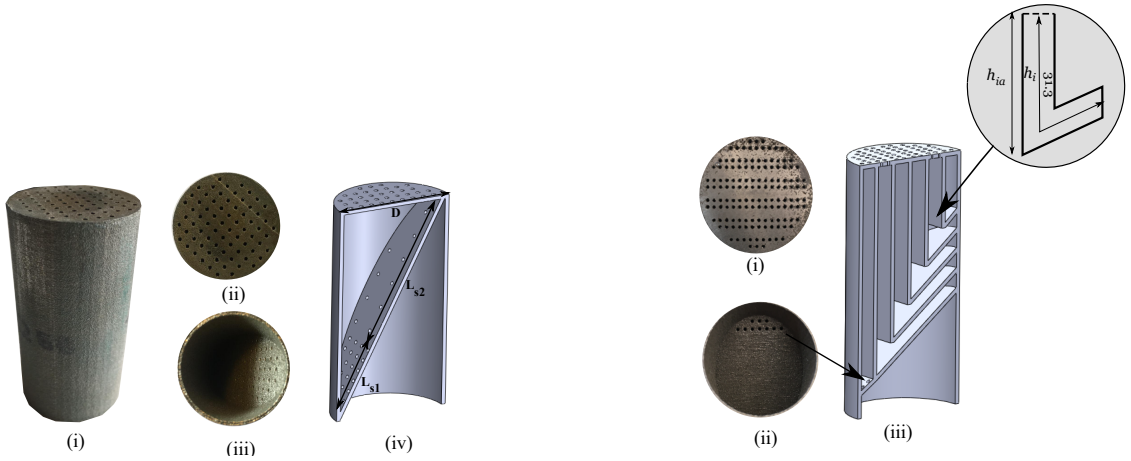

(a) Slanted septum core. **(b) MultiFOCAL.**

Fig. 2 3-D printed single cell cylindrical samples.

using the COMSOL FE model, to absorb sound over a relatively large frequency bandwidth. The cavity depth (Hc) of the novel liners is set nominally to 60 mm in order to minimise the space requirement of the acoustic liners installed inside a turbofan nacelle. The acoustic properties of the liner are predicted using a numerical impedance tube model developed in COMSOL [17]. Semi-empirical impedance equations for perforated sheets [21] are used in the FE model, initially without grazing flow, in the form of interior impedance boundary conditions given by

$$\frac{Z}{\rho_0 c_0} = \frac{\alpha \mu t_p}{2\rho_0 c_0 \left(\sigma C_D\right) {d_h}^2} + \frac{1-\sigma^2}{2c\sigma^2 C_D^2}|\hat{u}| + \mathrm{i}\,\frac{k(t_p + \epsilon\gamma d_h)}{\sigma}, \tag{1}$$

Table 1 The depth of each segments of MultiFOCAL and the corresponding first quarter-wave (QW) resonance frequency.

Cavity	Depth (h_i), mm	First QW Frequency, Hz
1	79.8	1065
2	75.3	1131
3	60.6	1405
4	45.9	1856
5	31.3	2721
6	14.7	5794

where α is an empirical constant, $|\hat{u}|$ is the surface acoustic particle velocity component normal to the perforated plate, μ is the dynamic viscosity of air, t_p is the facing sheet thickness, ρ_0 is the density of air, c_0 is the speed of sound, σ is the percentage open area ratio of the facing sheet, C_D is the discharge coefficient, d_h is the facing sheet perforate hole diameter, and γ is the dimensionless non-linear correction for reactance deduced by Murray and Astley [21] using high amplitude impedance tube measurements.

For perforates, the dimensionless Ingard end correction (ϵ) at low SPL is given by [22]

$$\epsilon = 0.85(1 - 0.7\sqrt{\sigma}). \tag{2}$$

An automated hybrid optimisation procedure is used to determine the optimum percentage open areas of the novel intake liners without grazing flow [23]. The average normal incidence sound pressure reflection coefficient for a given frequency range is used as the cost function, and it is evaluated by using the numerical impedance tube test model. The initial acoustic calculations were performed using the COMSOL FE model where a pure tone plane wave is incident normally on the liner surface with SPL = 150 dB, representative of the sound pressure level in the intake of a large high bypass ratio engine at high power settings.

The percentage open area (POA) of the liner facing sheet and the septum are constrained within the range of 1 % (almost hard wall) to 20 % (approaching zero acoustic impedance). In this optimization, the hole diameter and the thickness of the facing sheet and the diagonal layer are chosen to cover the range of interest applicable for aero-engine nacelles. The novel liner concepts were optimized initially for maximum sound absorption at normal incidence. The optimum solutions were searched using the *Genetic Algorithm (GA)* and *fmincon* for single objective calculations, and *gamultiobj* for multi-objective calculations, in MATLAB [24]. The total number of populations and generations were set to 100 and 3, respectively. With a large population size, the genetic algorithm searches the solution space thoroughly, thereby reducing the chance that the algorithm returns a local minimum that is not the global minimum.

IV. Prediction and measurement of normal incidence impedance

In this section, the impedance spectra of the SSC and the MultiFOCAL concepts are predicted and measured without grazing mean flow. Equation 1 is used along with the COMSOL FE model to predict the impedance spectra for each liner, and these spectra are compared with those measured using the HBK high intensity portable impedance meter. The impedance spectra are measured using broadband excitation at facing sheet OASPLs between 130 dB and 150 dB, increasing in 5 dB steps. In all of the results presented in this section, the pure tone predictions were performed at a targeted sound pressure level on the facing sheet of the liner, for frequencies between 100 Hz and 6000 Hz, in 100 Hz steps. Comparisons of measured and predicted impedance spectra are used to assess the accuracy of the prediction model.

A. Slanted Septum Core

Fig. 3 shows the comparisons of the predicted pure tone (+ symbols) and the measured broadband response (solid lines) of the Slanted Septum Core (SSC) with variable open area (**Fig. 2a**). The broadband optimum design solution, σ_{fs} = 10.3 %, σ_1 = 8.6 % and σ_2 = 1.6 %, has been found based on the criterion of maximum allowable average

coefficient of reflection $\bar{\tau}_{1,2} \leq 0.2$, in the frequency ranges (0.4–1 kHz and 2–6 kHz). The details of the design and the optimisation of the SSC liner is reported in a separate paper [23]. An initial observation from the impedance spectra is

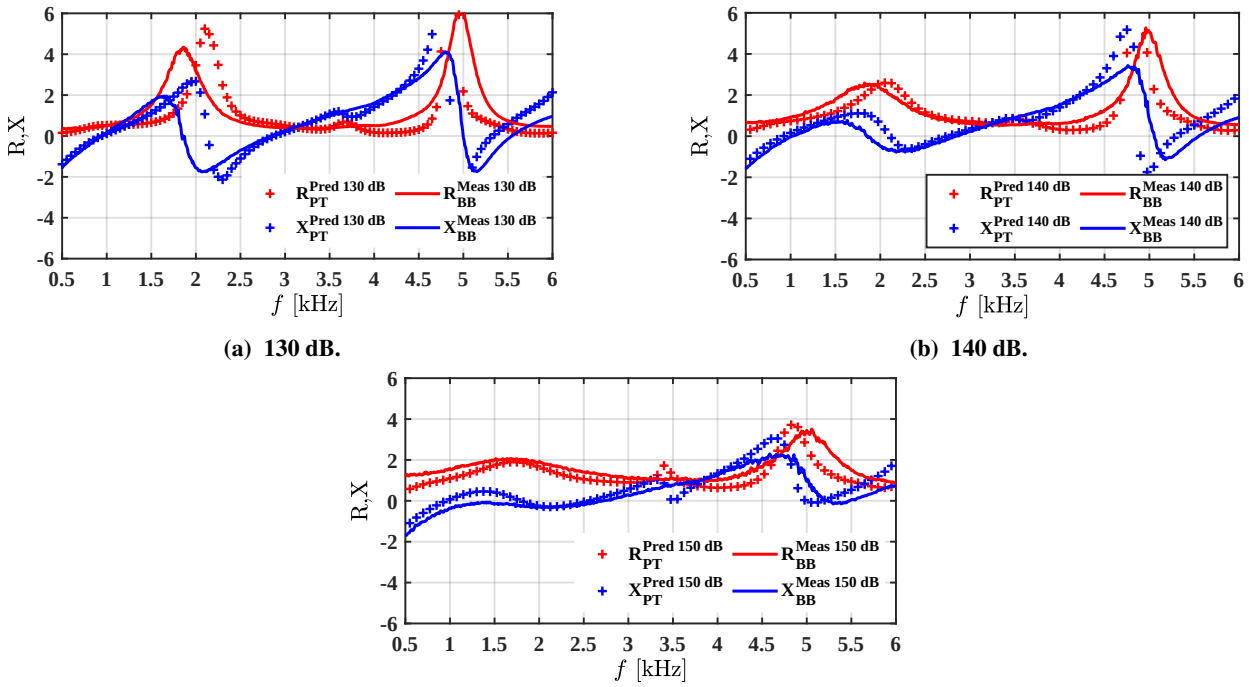

(a) 130 dB. **(b) 140 dB.**

(c) 150 dB.

Fig. 3 Acoustic properties of SSC liner optimized for broadband frequency sound absorption. Pure tone predictions (symbols), broadband excitation measurements (solid lines). Resistance (red color) and Reactance (blue colour).

that the pure tone prediction shows good agreement with the broadband measured data for all but the frequencies near anti-resonances. Furthermore, as expected, as the SPL increases, the resistance increases and the reactance decreases. Another observation is the slight shift in the anti-resonance frequency. **Fig. 3a** shows the comparison of the predicted and the measured acoustic impedance spectra of the SSC at 130 dB. As mentioned previously, the resistance (red) and reactance (blue) are normalised by the characteristic impedance of air $\rho_0 c_0$. The normalised reactance of this liner configuration crosses zero (towards positive values) at 920 Hz, 2800 Hz, and 5200 Hz, seen in **Fig. 3a**. Also, from the pure tone prediction, anti-resonances can be seen at 2100 Hz and 4700 Hz.

Similarly, **Fig. 3b** and **Fig. 3c** show the comparison of the predicted and the measured impedance spectra at 140 dB and 150 dB, respectively. Comparing the impedance spectra at 130, 140, and 150 dB highlights the significant impact of sound pressure level on the acoustic properties of the SSC liner. The total resistance of the SSC at 150 dB is approximately 0.5 to 1.0 $\rho_0 c_0$, for frequencies away from the anti-resonances, higher than the corresponding values at 130 and 140 dB. Also, there is a clear evidence of damping of the anti-resonances at higher SPLs, with the "flattening" of the reactance leading to improved absorption at higher frequencies.

Fig. 4 shows a comparison of the normal incidence sound absorption spectra between the pure tone predictions and the broadband measurements for 140 dB source excitation. With the optimum broadband design solution, a sound absorption coefficient of at least 0.8 is achieved in the frequency range of 500 to 3800 Hz. The absorption coefficient decreases gradually to reach a minimum value of 0.4 and 0.2 for broadband and pure tone excitation, respectively. This is due to the presence of an anti-resonance at around 4700 Hz, which represents one-and-a-half wavelengths for the longest sound propagation path length. It is important to note that in addition to providing a longer propagation path length at lower frequencies, the porous layer 2 helps to improve the overall panel absorption by acting as a complex DDOF liner at higher frequencies. As a result of this, the frequencies for maximum absorption in the pure tone spectra are at 920 Hz, 2800 Hz, 3700 Hz and 5200 Hz, where the normalised resistance and reactance values approach 1 and 0, respectively. Again, even considering the difference in source content, the agreement between the measurements

and the predictions is very good, except for a slight shift in the absorption spectrum around the third and fourth peak absorption frequency. This can be due to the simplification of the sound source model from broadband to pure tone in the numerical calculation. The corresponding mismatch between the predicted and measured impedance at high frequency is seen in Fig 3b.

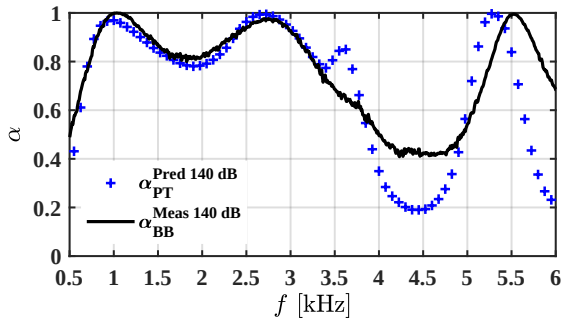

Fig. 4 Comparison of absorption coefficient of the slanted septum core for broadband measurements (black line) and pure tone predictions (blue +) at 140 **dB.**

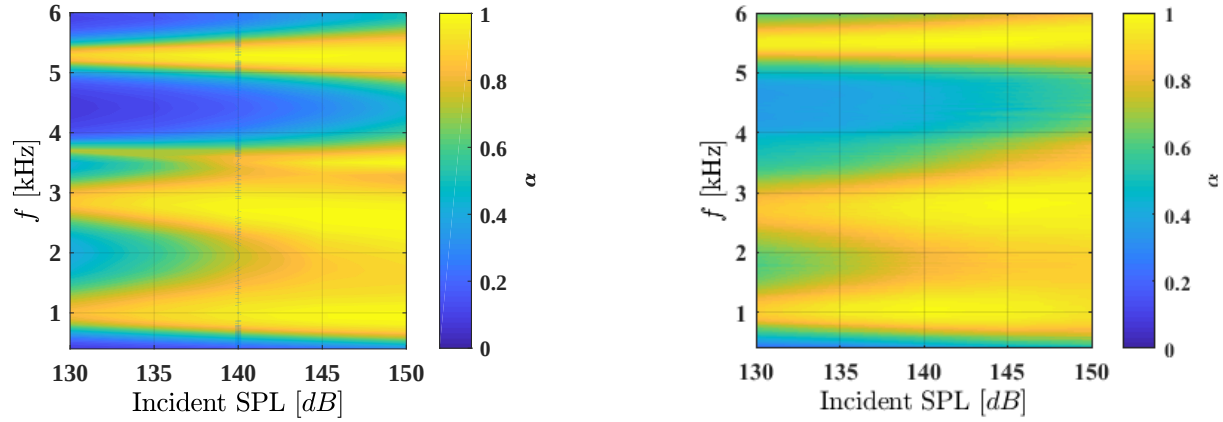

(a) Predictions - Pure tone excitations. **(b) Measurements - Broadband sound excitations.**

Fig. 5 Absorption coefficient contour of slanted septum core.

Fig. 5 presents the absorption coefficient spectra as a function of incident sound pressure level in the (SPL,f)-plane for pure tone (**Fig. 5a**) and broadband (**Fig. 5b**) excitation. The incident sound pressure level increases from 130 dB to 150 dB, and excitation frequency varies between 400 and 6000 Hz. The chosen range of SPL and frequency covers typical values relevant to aircraft engine duct applications. The common observation between **Fig. 5a** and **Fig. 5b** is that the absorption coefficient bandwidth of the SSC improves significantly with increasing excitation SPL. The anti-resonances at 2100 Hz and 4700 Hz, which are clearly noticeable at 130 dB, are significantly damped at 150 dB. It is observed that the frequencies for peak absorption vary little and the width broadens with increasing SPL. This is a benefit of the increased non-linear resistance provided by the perforated layer 2. Also, there is good agreement between the absorption for pure tone predictions and the broadband measurements. Overall, the SSC liner performs well over a broad range of frequencies at high SPL. It is noted, however, that the wide broadband target is difficult to achieve at all frequencies with this design, as evidenced by the dip in absorption at around 4300 Hz.

B. MultiFOCAL

Fig. 6 shows the comparison of the measured broadband impedance spectra of the MultiFOCAL liner geometry, optimised using pure tone predictions. The optimum percentage open area of the facing sheet of segments 1–6 is 19 %

and the septum of segment 1 is 11.3 %. In **Fig. 6a**, for pure tone excitation at 130 dB, the normalized reactance is close

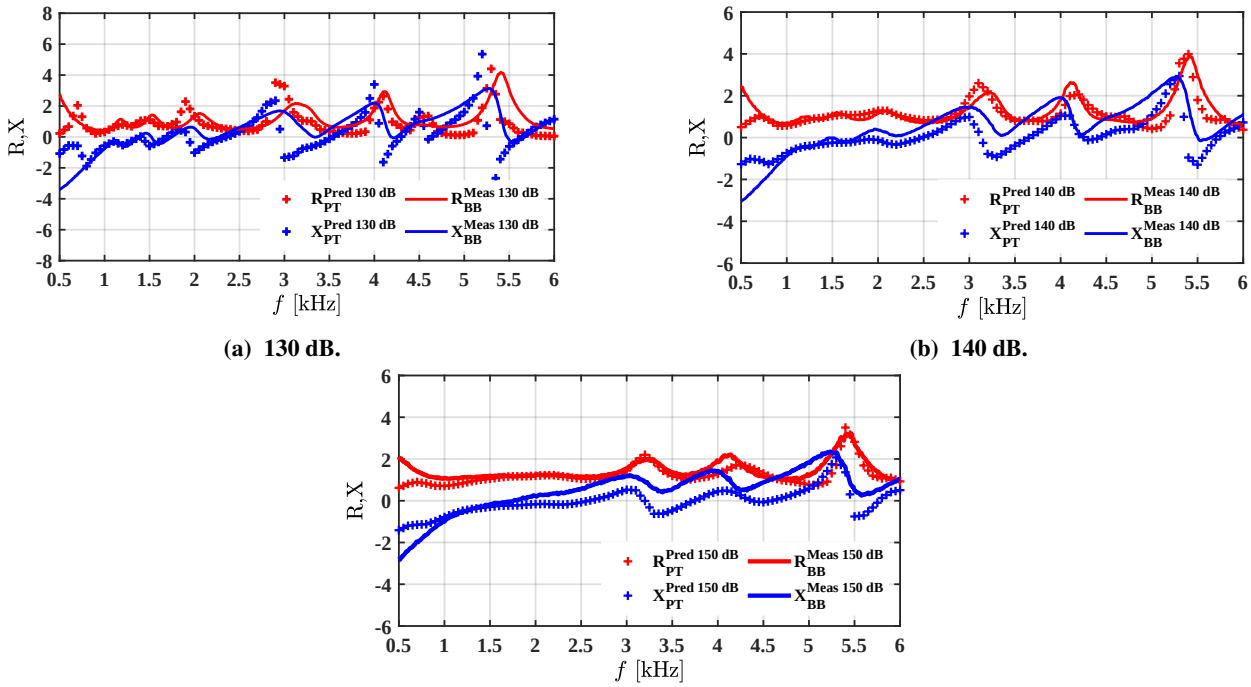

(a) 130 dB. **(b) 140 dB.**

(c) 150 dB.

Fig. 6 Predicted and measured impedance spectra of MultiFOCAL concept. Resistance (red color), Reactance (blue color), Broadband source type measurements (solid lines), and Tonal source type predictions (symbols).

to zero for most of the frequencies in the range of 0.9 to 5.3 kHz given the combination of six folded cavities with different depths. The resistance of the liner surface is mainly controlled by the septum (septum 1) of segment 1, in addition to the perforated facing sheets. This is because the optimum percentage open area of septum 1 is low compared to the facing sheet of segments 1–6. Therefore, the septum has a greater non-linear resistance component at high SPLs.

As in the case for the SSC, comparing the impedance spectra at 130, 140, and 150 dB highlights the influence of the sound pressure level on the acoustic properties of the MultiFOCAL configuration. The total resistance of the MultiFOCAL at 150 dB is close to 1.0 $\rho_0 c_0$, for frequencies away from anti-resonances, higher than the corresponding values at 130 dB. Also, there is again clear damping of anti-resonances with increasing sound pressure level irrespective of the source type. Therefore, at 150 dB (**Fig. 6c**), the six closely packed peaks are broadened due to the general increase in the resistance, damping of the anti-resonances, and flattening the normalised reactance curve towards zero.

Figs. 7 shows the comparison of the measured and the predicted normal incidence absorption coefficient spectra of the MultiFOCAL concept at increasing SPL, for frequencies between 0.5 kHz and 6.0 kHz. For the pure tone predictions at 130 dB (**Fig.7a**), the first absorption peak is located at 0.7 kHz and the absorption coefficient is above the target value of 0.8. Although the panel's normalised reactance is close to zero, the normalised resistance is $\approx 2\rho_0 c_0$. The additional peaks in the absorption spectra are located at 1.4, 1.8, 2.3, 3.3, 4.3, 4.6, and 5.5 kHz, where the panel's normalised reactance is close to zero. Also, there are three dips, between 2.3 and 5.7 kHz, in the predicted absorption spectra at 2.8, 3.8, and 5 kHz at 130 dB.

The measured absorption coefficient spectra shows good agreement with the predictions for the majority of the frequencies between 0.9 and 6 kHz at 130 dB. Also, it can be seen that a high absorption coefficient (greater than 0.8) is maintained over a wide frequency band (0.9–5.0 kHz) at 150 dB. The small difference between the measured and predicted spectra can be attributed to variations in the facesheet and the septum hole dimensions from the nominal values, due to the 3-D printing process. Additionally, the simple 2-D numerical model exceeds the measured absorption coefficient. Comparing the predicted and measured impedance spectra in **Fig. 6**, this may arise from increased inertance in the manufactured facing sheets. Nevertheless, the agreement is sufficiently close to provide confidence in the proposed liner geometry and the prediction model.

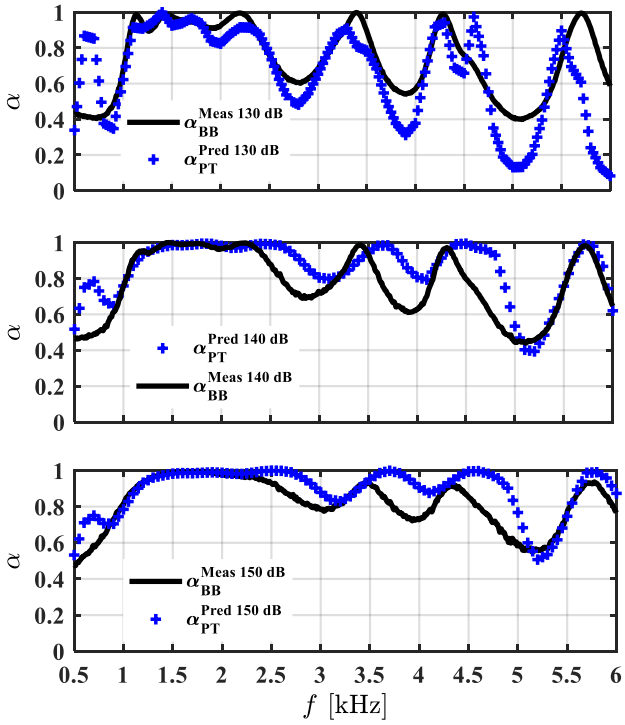

Fig. 7 Comparison of measured absorption coefficient spectra of the MultiFOCAL concept for broadband excitations with pure tone predictions. a.) 130 **dB, b.)** 140 **dB, and c.)** 150 **dB.**

V. Validation of the grazing flow numerical model

The COMSOL FE modelling of sound propagation in a lined flow duct used in this work has been validated by comparing the measured in-duct insertion loss of a single-degree-of-freedom (SDOF) linear liner with the numerical predictions. The experimental data, previously tested by the NLR, are reported in Murray et al. [12]. The dimensions of the lined section and the SDOF liner is presented in Table2. The acoustic properties of the liner under this study

Table 2 Geometrical parameter of the linear SDOF liner

Type	Panel Geometry	Facing Sheet	Cell Depth (mm)
Single Layer Linear	850 mm × 170 mm	Linear wire mesh	30.5

is predicted by pure tone excitation at a sound pressure level of 130 dB and for frequencies up to 6 kHz, using the measured values from [12] as a guide. The predicted impedance spectra is shown in **Fig. 8a**.

Fig. 8b shows the comparison between the predicted and the measured insertion loss of the SDOF linear liner with zero grazing flow. As mentioned previously, at the source plane, the incident sound field is multi-modal comprised of all propagating radial modes with zero azimuthal order $m = 0$. The sound powers W_{in} and W_{out} are the sum of acoustic power at the respective inlet and outlet reference planes. The insertion loss is calculated from the difference between the in-duct power transmission loss with and without liner and given by,

$$\mathrm{IL} = \Delta_{\mathrm{PWL}}^{\mathrm{With\ liner}} - \Delta_{\mathrm{PWL}}^{\mathrm{Without\ liner}}. \tag{3}$$

Good agreement between the prediction and the measurement is observed. The insertion loss peaks at 1300 Hz as the impedance of the SDOF liner around this frequency approaches the optimum wall impedance. The insertion loss achieved by the liner then decreases gradually with increasing frequency and at 5500 Hz the predicted insertion loss is almost zero due to the anti-resonance of the liner.

Fig. 9 shows the comparison between the predicted and measured broadband sound power insertion loss spectra of the SDOF linear liner with mean flow. For downstream sound propagation, in **Fig. 9a** and **Fig. 9c**, it can be seen that

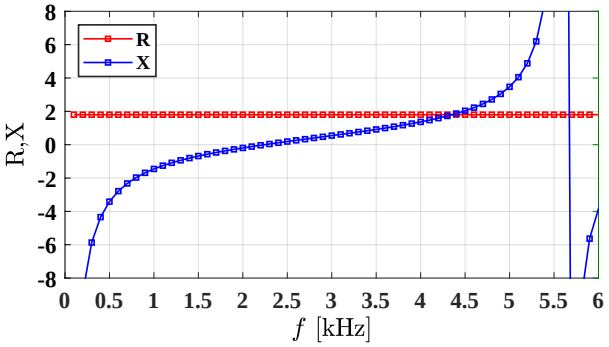

(a) Predicted acoustic properties of SDOF linear liner.

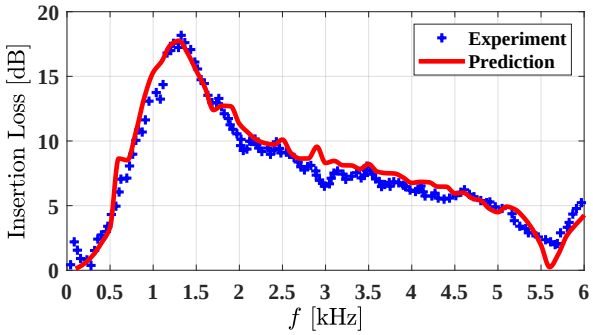

(b) Comparison between prediction and measurement.

Fig. 8 Insertion loss of SDOF linear liner at M=0.

there is good agreement between the prediction and the measurement at Mach 0.3 and 0.5. This suggests that a simple model of the broadband noise source with the assumption of: (1) uncorrelated cut-on radial modes ; (2) propagating radial modes carry equal energy per mode, along with the standard Ingard–Myers boundary condition can accurately predict the acoustic performance of liners using a uniform mean flow approximation. Around 5500 Hz, there is a slight disagreement between the prediction and the measurement. This is due to the increase in the local value of normalised resistance as measured seen when using an impedance meter (**Fig. 7 in [12]**).

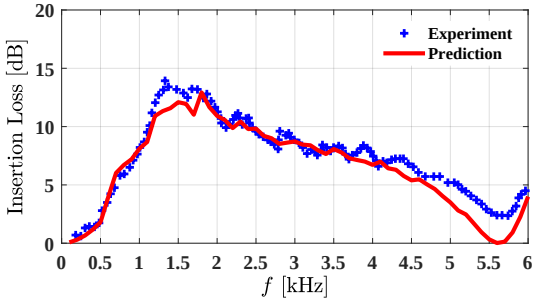

(a) Downstream flow at 0.3 Mach.

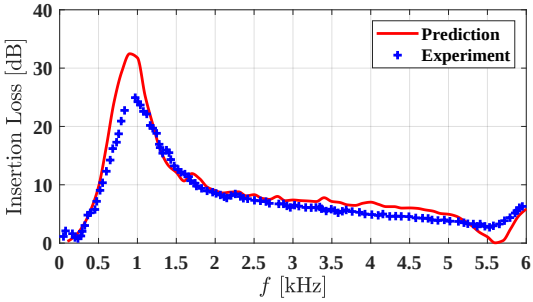

(b) Upstream flow at 0.3 Mach.

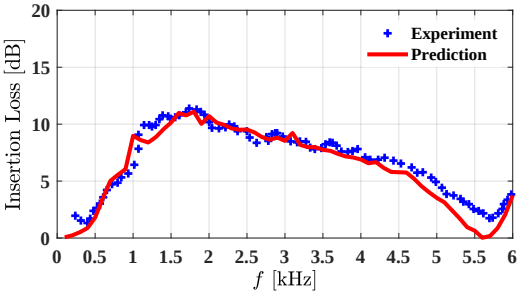

(c) Downstream flow at 0.5 Mach.

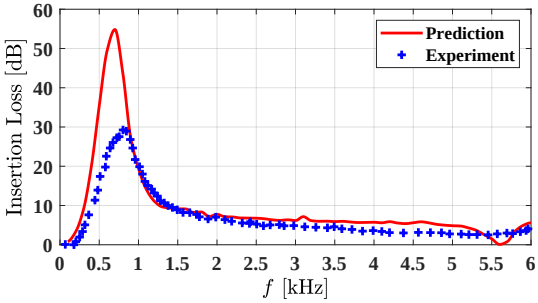

(d) Upstream flow at 0.5 Mach.

Fig. 9 Broadband insertion loss comparison between prediction and measurement of SDOF linear liner with mean flow.

For upstream propagation, in **Fig. 9b** and **Fig. 9d**, the broadband insertion loss predictions with a uniform flow approximation are generally too high, especially around the peak value. For instance, at Mach 0.3 and around 970 Hz the difference between the predicted and the measured insertion loss is approximately 8 dB. The discrepancy increases with increasing Mach number (see **Fig. 9d**). This discrepancy between measurement and prediction for the case of upstream sound propagation is attributed to the absence of the boundary layer in the numerical model; this observation is consistent with the previous results reported by Gabard [10, 25]. Also, the shift in the frequency of peak attenuation

can be seen by comparing the downstream and upstream spectra; this is due to the influence of the grazing flow direction and Mach number on the optimum wall impedance.

A. NLR flow duct optimum impedance

Fig. 10 presents a subset of the insertion loss contours for downstream propagation as a function of normalised resistance and reactance for a given excitation frequency, at varying Mach numbers, based on the lined test section in the NLR flow duct test facility. It is observed from **Figs. 10a**, **10c** and **10e** that with increasing frequency, from 500 Hz to 4000 Hz, the optimum resistance increases, the reactance decreases, and the maximum attainable insertion loss reduces. Also, the maximum possible insertion loss is achieved at low frequencies where the modulus of optimum resistance and reactance are very low. In **Figs. 10b**, **10d** and **10f** the equivalent insertion loss contour plots are shown for M=+0.3. The optimum wall impedance, and the respective maximum possible insertion loss at each frequency and Mach number, are summarised in **Fig. 11**. It is seen that the moduli of the optimum resistance and reactance reduce with increasing positive flow, while the maximum possible attenuation decreases (consistent with the results of [9]).

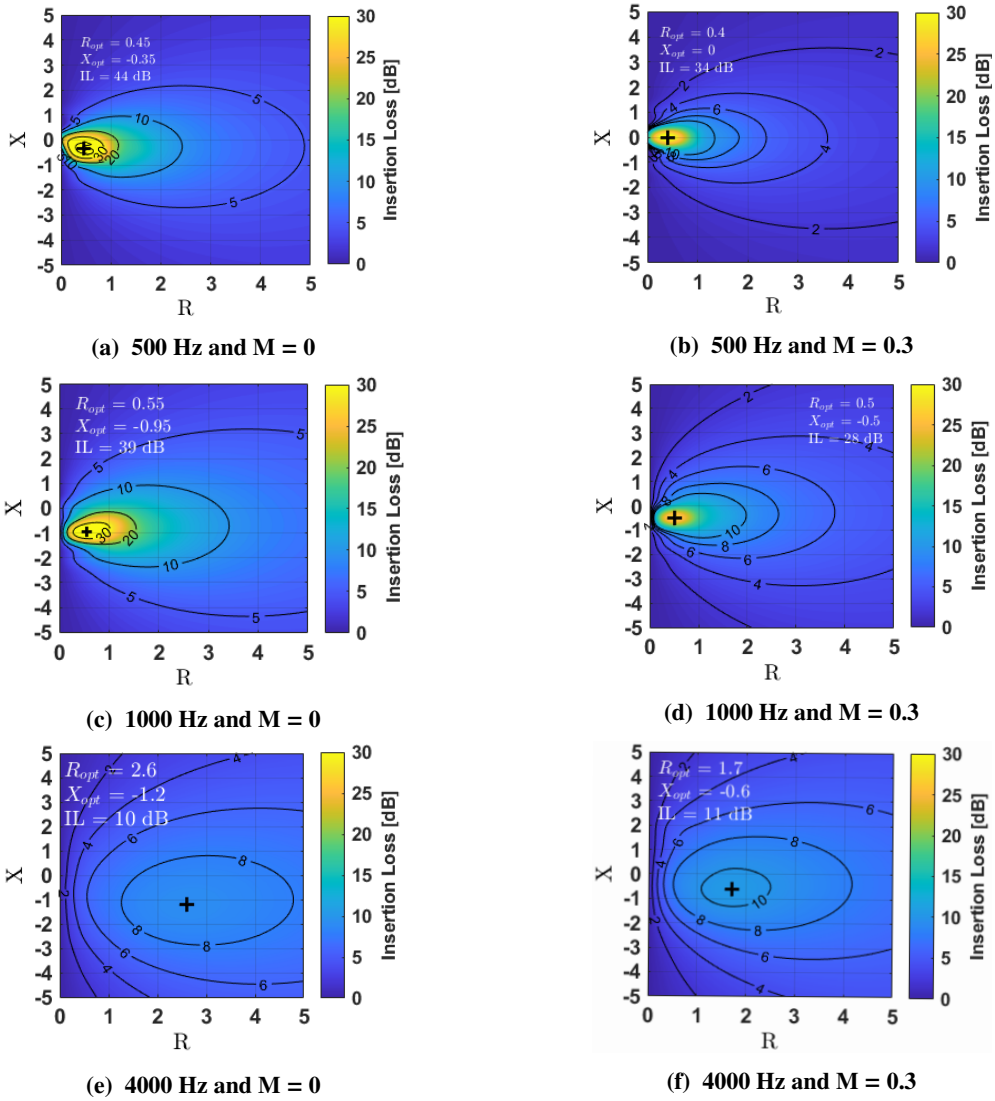

(a) 500 Hz and M = 0

(b) 500 Hz and M = 0.3

(c) 1000 Hz and M = 0

(d) 1000 Hz and M = 0.3

(e) 4000 Hz and M = 0

(f) 4000 Hz and M = 0.3

Fig. 10 Insertion loss contour plots

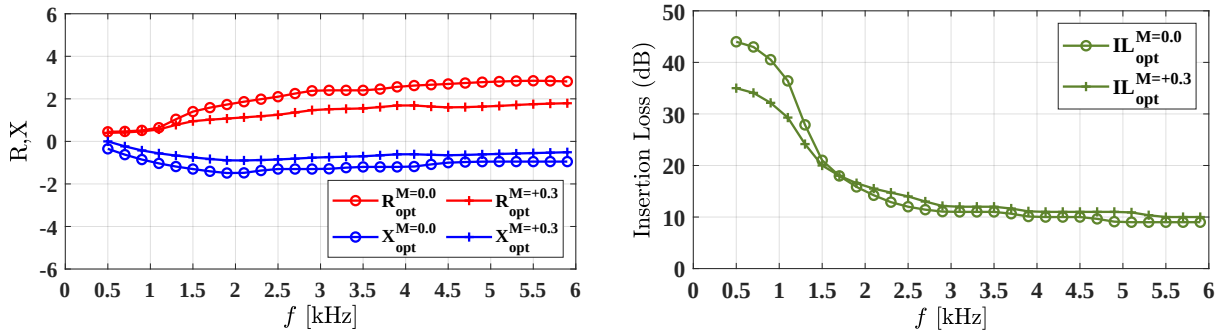

(a) Optimum impedance at M = 0 and +0.3. **(b) Maximum possible insertion loss at M=0 and +0.3.**

Fig. 11 NLR flow duct facility optimum impedance and maximum possible insertion loss.

VI. Prediction of insertion loss for novel liners

The SSC and MultiFOCAL liners were optimized at Mach 0.3 for downstream propagation. In the future, it is planned to manufacture these liner configurations and measure the insertion loss in the NLR flow duct test facility, for both downstream and upstream propagation, at Mach numbers ranging from 0.0 to 0.7. The results will be reported in a follow-up paper.

The predicted performance of the novel liners in the NLR duct are presented at Mach 0 and 0.3 for downstream propagation, since the absence of a boundary layer in the potential flow model is expected to have negligible impact on the results for downstream propagation. The aforementioned follow-up paper will also present predictions for upstream propagation which will account for boundary layer refraction.

A. No flow condition

In **Fig. 12**, the predicted pure tone impedance of the SSC and MultiFOCAL liner concepts at 140 dB (**Fig. 3b** and **Fig. 6b**), are compared with the NLR duct optimum impedance for the no grazing flow condition. From **Fig. 12a**, for frequencies between 0.5 kHz and 1 kHz, it can be seen that the normalised resistance of the slanted septum core is almost equal to the NLR duct optimum resistance. On the other hand, the resistance of the MultiFOCAL is close to the NLR duct optimum resistance at 0.5 kHz (0.45 $\rho_0 c_0$) and it tends to increase to 1.0 $\rho_0 c_0$ at 0.7 kHz. Although an increase in resistance towards 1.0 $\rho_0 c_0$ is desirable for normal incident sound waves, the optimum resistance in the NLR duct is very different from that at normal incidence. As frequency increases above 1 kHz, the novel liner resistance oscillates, with the quality of the match to the NLR optimum reducing with increasing frequency.

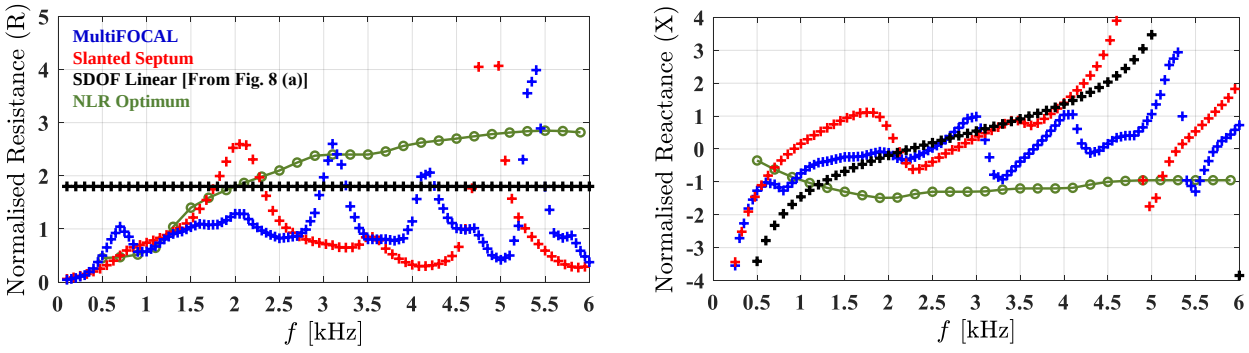

(a) Normalised resistance. **(b) Normalised reactance.**

Fig. 12 Comparison between the SSC and the MultiFOCAL concepts for pure tone excitation at 140 dB without grazing flow.

Similarly, the comparison of normalised reactance is shown in **Fig. 12b**. It can be seen that the reactance of both of

the liner concepts are comparable to the NLR duct optimum at only a few selected frequencies. However, the novel liner reactances of these 60 mm deep configurations cross-over the optimum at low frequencies, and remain closer to the optimum over a large range of frequencies that would not be possible with a traditional single-layer configuration. For example, the reactance of the SSC is comparable to the NLR duct optimum at 700 Hz, while the reactance of the MultiFOCAL is comparable at 920 Hz. It should be noted that designing a liner with a reactance spectrum matching the NLR duct optimum (or any duct optimum) over a large frequency bandwidth is not a straightforward task.

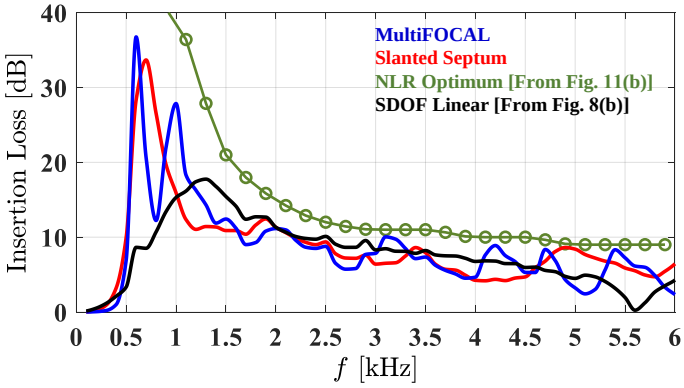

Fig. 13 Predicted broadband sound power insertion loss of novel liners at M = 0.

The insertion loss performance of the SCC and the MultiFOCAL liner concepts are predicted and compared in **Fig. 13**. It is reminded that the COMSOL FE model is based on an annular duct. At the source plane, the incident sound field is multi-modal with azimuthal order zero ($m = 0$). As the frequency increases, progressively higher-order radial modes are cut on and propagate. The predicted insertion loss of the conventional SDOF linear liner, which is shown in **Fig. 8b**, is also plotted in this figure for reference. As expected, at lower frequencies, both of the novel liner panels show a significant improvement in the predicted insertion loss below 1000 Hz, given the improved match to the optimum impedance (see **Fig.12**). The insertion loss of the SSC panel has a peak (33 dB) at 700 Hz. The MultiFOCAL panel has two peaks in the spectrum between 500 and 1000 Hz. The first peak occurs at 600 Hz and second peak at 980 Hz with an insertion loss of 37 dB and 28 dB, respectively. The insertion loss of the MultiFOCAL drops at frequencies around 800 Hz. This is consistent with a reduced quality impedance match with the optimum. It is noted that at low frequencies (see **Figs. 10a** and **10c**) there are large changes in the insertion loss contour levels in the vicinity of the maximum value, thus the insertion loss will be very sensitive to any uncertainty in the predicted impedance or the insertion loss modelling. Also, it can be seen in **Fig. 13**, that the maximum possible insertion loss is more sensitive to a given variation in impedance at lower frequencies compared to higher frequencies.

The novel liners provide large gains over the SDOF linear liner at frequencies below 1000 Hz. For frequencies between 1000 Hz and 6000 Hz, both of the liner panels provide an insertion loss of at least 5 dB. The insertion loss performance of the novel liners is similar to that of the SDOF linear liner up to 4.5 kHz, and it shows additional gains at higher frequencies in the region of the anti-resonance of the SDOF linear liner.

B. Liner re-optimisation for downstream propagation at Mach 0.3

The percentage open areas of the SSC and MultiFOCAL liners were re-optimised at Mach 0.3 for downstream propagation using an automated hybrid global optimisation procedure in MATLAB [24]. In this optimisation, the open area of the liner facing sheet and the septum were constrained within the range of 1 % (almost hard wall) to 30 % (approaching zero acoustic impedance). The hole diameter and sheet thickness were set to 0.8 mm and 1 mm, respectively. The optimum solutions were searched using the *Genetic Algorithm (GA)* and *fmincon* for single objective calculations in MATLAB [24]. The total number of populations and generations were set to 100 and 3, respectively.

It was observed during this re-optimisation study that choosing an objective function targeting NLR duct optimum impedance, for such complex geometries, causes strong oscillations in the reactance curve due to anti-resonances. As a result, the corresponding insertion loss of the liner had many dips in the spectrum. To overcome this, the average reduction in acoustic power for a given frequency range was used as the objective function. First, for a set of open areas from the population and, at a given tonal frequency, the impedance predictions were performed using the normal

incidence COMSOL FE model where a pure tone plane wave was incident normally on the liner surface with a sound pressure level of 140 dB at Mach 0.3. Then, the predicted resistance and reactance was used to find the respective insertion loss value from the R-X contour plot (see for example **Figs. 10b**, **10d** and **10f**). The resolution of the R-X values in the contour plot was refined, using a cubic spline data interpolation function in MATLAB [24], to improve the search operation. The insertion loss for the impedance values outside of the R-X range ($0 \leq R \leq 5$ and $-5 \leq X \leq 5$) was assumed to be zero. Then, the insertion loss curve for a specific set of open areas was averaged over a targeted frequency bandwidth. No weighting was applied to the objective function.

The optimum solutions of the SSC, MultiFOCAL, and SDOF liners, for different frequency regimes are summarised in **Table. 3**. In this paper, prediction results are compared for the highlighted cases only. Except for the MultiFOCAL concept, all of the liners in Table.3 were optimised with mean flow (Mach = 0.3) at 140 dB. This is because the optimum design solution of the MultiFOCAL with and without mean flow provided similar predictions of the panel's impedance and insertion loss. The facing sheet open area of the SSC 4 was set equal to 20 % as it would be difficult to manufacture a facing sheet with such a high POA using 3-D printing. The insertion loss for this corrected design (SSC 4.1) was predicted and compared to the original design (SSC 4). There was no significant difference in the insertion loss. It is planned that the liner configurations SSC 4.1 and the MultiFOCAL will be manufactured and tested in the NLR grazing flow test facility, for both downstream and upstream propagation, at Mach numbers ranging from 0 to 0.7.

Table 3 Optimised liner designs (results of the highlighted designs are discussed in this paper)

Liner Type	Frequency Range (kHz)	Facing Sheet POA (%)	Septum 1 POA (%)	Septum 2 POA (%)	Cavity Depth (mm)
SDOF(Perforate)	0.5 - 6	10.3	-	-	75.2
SDOF(Perforate)	1.5 - 6	5.4	-	-	13.4
SDOF(Wire mesh)	0.5 - 6	Linear design	-	-	57.8
SDOF(Wire mesh)	1.5 - 6	Linear design	-	-	16.8
SSC 1	0.5 - 6	13	1	6.8	60
SSC 2	1.5 - 6	12.3	2.4	2.9	20
SSC 3	1.5 - 6	24.6	8.4	1.5	40
SSC 4	1.5 - 6	28.6	3.2	1.5	60
SSC 4.1	1.5 - 6	20	3.2	1.5	60
SSC 5	3 - 6	12.4	2.3	2.7	20
SSC 6	3 - 6	24.2	8.6	3	40
SSC 7	3 - 6	29.6	2.3	5.8	60
MultiFOCAL	0.5 - 6	19	11.3	-	60

C. Downstream propagation at Mach 0.3

As stated earlier, the novel liners were optimized for the Mach 0.3 downstream propagation condition. For all of the predictions presented in this section, the grazing mean flow is assumed to be uniform. First, for both of the liner configurations, the impedance values have been adjusted for the effect of grazing flow using the semi-empirical model reported in the literature [21, 22]. Therefore, similar to the case of a classical SDOF liner with perforated face-sheet, the flow leads to an increase in the overall resistance of the liner panel. **Fig. 14** shows the comparison of the predicted pure tone response, for Mach 0.3 at 140 dB, for the SSC 4.1 and the MultiFOCAL concepts. The predicted impedance is compared with the NLR duct optimum impedance for Mach 0.3. The optimum resistance reduces relative to that seen at zero grazing flow (particularly at higher frequencies), while the optimum reactance moves a little closer to zero.

From **Fig. 14a**, it can be seen that, at lower frequencies (500 Hz to 1200 Hz), the normalised resistance of the SSC 4.1 is closer to the duct optimum than the MultiFOCAL. However, at higher frequencies (above 1200 Hz), the trend reverses, as the normalised resistance of the MultiFOCAL, on average, is slightly closer to the duct optimum. Comparison of **Fig. 14a** with **Fig. 12a** shows that the acoustic resistance increases for both of the liner configurations, with the largest increase mainly seen at low frequencies. This is consistent with the observations previously reported by Murray and Astley [21] for a SDOF liner with a perforated facing sheet.

As is the case with zero flow(**Fig. 12b**), **Fig. 14b** once again shows that it is difficult to match the reactance spectrum of both of the novel liners to the duct optimum over a wide range of frequencies. However, the overall reactance of

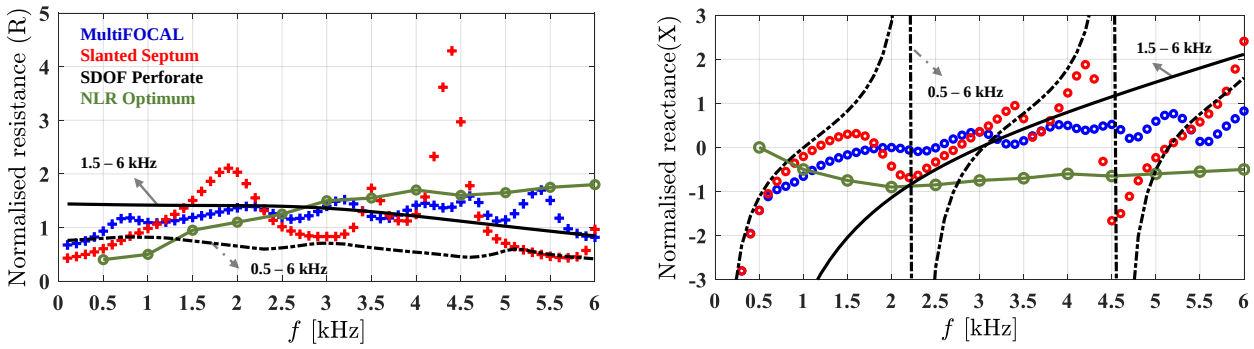

(a) Normalised resistance. **(b) Normalised reactance.**

Fig. 14 Impedance spectra comparison between the SSC 4.1 and the MultiFOCAL concept for pure tone excitation at 140 dB and Mach 0.3.

the novel concepts decreases with grazing flow which improves the reactance match to the optimum. This is due to a reduction in the facing sheet reactance component.

Fig. 15 shows the predicted in-duct power loss of the SSC and the MultiFOCAL concepts. For comparison, an SDOF perforate configuration, optimised for maximum insertion loss, is also included for two different frequency regimes. The SDOF perforate liner optimised in the frequency range of 1.5 kHz to 6 kHz, marked by the solid black line, is shallower (cavity depth). As a result, it can be seen from the corresponding insertion loss plot that the performance of this liner is poor below 1 kHz. However, the anti-resonance of this shallow SDOF perforate liner is outside of the targeted frequency range, thus there are no dips in the insertion loss below 6 kHz. On the other hand, the SDOF perforate liner optimised in the frequency range of 0.5 kHz to 6 kHz has a deeper cavity depth; therefore, the corresponding insertion loss of this liner has two dips, at 2.3 kHz and at 4.6 kHz, in the targeted frequency range.

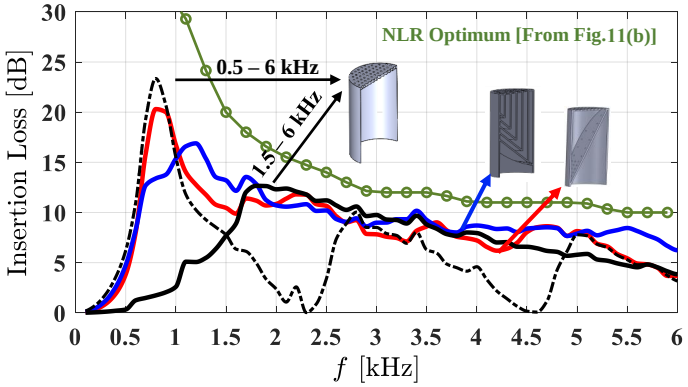

Fig. 15 Predicted insertion loss of SSC 4.1, MultiFOCAL, and conventional SDOF perforate liner at Mach 0.3.

It may be concluded that both novel liner concepts provide significant improvements in attenuation when compared with an optimised SDOF perforate panel. The insertion loss peak has shifted towards higher frequency for both novel liner configurations compared to the no flow condition. This once again highlights the sensitivity of the insertion loss to small changes in optimum impedance at lower frequencies compared to higher frequencies.

Finally, a practical check on the application of the SSC concept is investigated by changing the maximum cavity depth (H_c). **Fig. 16** shows a comparison of the insertion loss obtained using a total cavity depth of 20 mm and 40 mm, along with the baseline depth of 60 mm. This corresponds to optimum solutions SSC 2, SSC 3 and SSC 4.1 in **Table. 3**. As described in Sec. VI.B, for each cavity depth, the porosity of the facing sheet and the slanted septum layers were optimised to achieve maximum insertion loss. As expected, a reduction in cavity depth can be seen to shift the insertion loss peak towards higher frequency. However, the SSC always provides a significant increase in insertion loss at lower

frequencies (below 1700 Hz) when compared against an optimised SDOF perforate (black line), while maintaining similar levels of attenuation at higher frequencies.

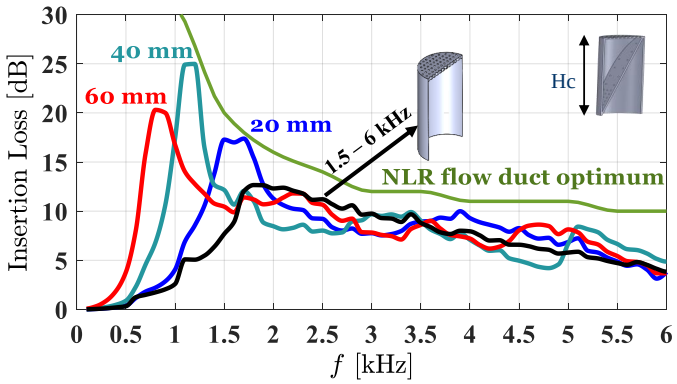

Fig. 16 Predicted insertion loss of the SSC concept for different cavity depths at Mach 0.3

VII. Conclusion

In this paper, the results from a detailed study into the broadband sound absorption performance of two novel liners are presented. First, the normal incidence impedance spectra of the SSC and the MultiFOCAL liner concepts are predicted and measured without grazing mean flow. A two-dimensional COMSOL FE model of a normal incidence impedance tube has been developed and used to predict the liner impedance. In the FE model, semi-empirical equations are applied as interior boundary conditions to translate physical parameters of the face sheet and septum into normalised resistance and reactance. The predicted normal incidence impedance spectra without grazing flow is shown to agree well with measurements, thus giving confidence in the modelling, manufacturability, and predicted performance of the proposed liner geometries.

Second, it has been shown that once the impedance spectrum is optimised for the no flow condition, it is then a relatively straightforward task to re-optimise the face sheet geometry in order to realise the desired liner impedance under grazing flow and incident sound field. A two-dimensional axisymmetric annular duct model of the NLR flow duct test facility has been modelled in COMSOL, and the in-duct insertion losses have been calculated based on a simple multi-modal sound source. For downstream propagation, the comparison of the predicted insertion loss of an SDOF linear liner with measurements shows that a simple model of the broadband noise source with the assumption of: (1) uncorrelated cut-on radial modes; (2) propagating radial modes carry equal energy per mode, along with the standard Ingard–Myers boundary condition, can accurately predict the acoustic performance of liners using a uniform mean flow approximation. However, for upstream propagation, more significant effects of sound refraction are seen in the prediction results for the SDOF linear liner. Additionally, it has been shown that the maximum possible insertion loss is more sensitive to small changes in impedance at lower frequencies compared to higher frequencies.

Finally, it has been shown that both liner concepts provide more attenuation, at lower frequencies, when compared against an optimised SDOF perforate liner at Mach 0.3, while maintaining similar levels of attenuation at higher frequencies. Also, it has been observed that the insertion loss peak is shifted towards higher frequency for both novel concepts in the presence of mean flow when compared to the no flow condition.

In future work, the insertion loss of novel liners will be analysed using measured flow profile parameters, including modelling the impact of boundary layer refraction. Further developments in the modelling also will include the implementation of a growing boundary layer profile over the liner surface, representative of the boundary layer measured in the NLR flow duct test facility. The predicted insertion loss of the novel liners will then be compared with measurements of the insertion loss acquired at the NLR flow duct test facility. Also, the behaviour of the MultiFOCAL liner under grazing flow will be investigated to identify the frequency when the lumped behaviour of the coupled cells separates into a local impedance.

Acknowledgments

The work in this article is part of the ARTEM project. This project has received funding from the European Union's Horizon 2020 research and innovation programme under grant No. 769 350. The authors wish to acknowledge the technical input to this work from Dr. Rie Sugimoto (ISVR), Prof. Jeremy Astley (ISVR) and Kylie Knepper (NLR). Also the authors wish to acknowledge the continuing support provided by Rolls–Royce plc through the University Technology Centre in Propulsion Systems Noise at the Institute of Sound and Vibration Research.

References

[1] Sugimoto, R., Murray, P., and Astley, R., "Folded Cavity Liners for Turbofan Engine Intakes," *18th AIAA/CEAS Aeroacoustics Conference*, 2012, pp. 1–13. https://doi.org/10.2514/6.2012-2291.

[2] Schiller, N. H., and Jones, M. G., "Smeared Impedance Model for Variable Depth Liners," *24th AIAA/CEAS Aeroacoustics Conference*, 2018, pp. 1–14. https://doi.org/10.2514/6.2018-3774.

[3] Nayfeh, A. H., "Effect of the acoustic boundary layer on the wave propagation in ducts," *The Journal of the Acoustical Society of America*, Vol. 54, No. 6, 1973, pp. 1737–1742. https://doi.org/10.1121/1.1914472.

[4] Nayfeh, A. H., Kaiser, E., J, and Shaker, S., B, "Effect of mean-velocity profile shapes on sound transmission through two-dimensional ducts," *Journal of Sound and Vibration*, Vol. 34, No. 3, 1974, pp. 413–423.

[5] Myers, M., "On the acoustic boundary condition in the presence of flow," *Journal of Sound and Vibration*, Vol. 71, No. 3, 1980, pp. 429 – 434.

[6] Ingard, U., "Influence of Fluid Motion Past a Plane Boundary on Sound Reflection, Absorption, and Transmission," *The Journal of the Acoustical Society of America*, Vol. 31, No. 7, 1959, pp. 1035–1036.

[7] Rienstra, S. W., and Darau, M., "Boundary-layer thickness effects of the hydrodynamic instability along an impedance wall," *Journal of Fluid Mechanics*, Vol. 671, 2011, pp. 559—-573. https://doi.org/10.1017/S0022112010006051.

[8] Brambley, E. J., "Well-Posed Boundary Condition for Acoustic Liners in Straight Ducts with Flow," *AIAA Journal*, Vol. 49, No. 6, 2011, pp. 1272–1282. https://doi.org/10.2514/1.J050723.

[9] Watson, W., and Jones, M., "Evaluation of Wall Boundary Conditions for Impedance Eduction Using a Dual-Source Method," *18th AIAA/CEAS Aeroacoustics Conference (33rd AIAA Aeroacoustics Conference)*, ???? URL https://arc.aiaa.org/doi/abs/10.2514/6.2012-2199.

[10] Gabard, G., "Boundary layer effects on liners for aircraft engines," *Journal of Sound and Vibration*, Vol. 381, 2016, pp. 30–47.

[11] Renou, Y., and Aurégan, Y., "Failure of the Ingard-Myers boundary condition for a lined duct: An experimental investigation," *The Journal of the Acoustical Society of America*, Vol. 130, 2011, pp. 52–60. https://doi.org/10.1121/1.3586789.

[12] Murray, P., Ferrante, P., and Scofano, A., "Influence of Aircraft Nacelle Acoustic Panel Drainage Slots on Duct Attenuation," *13th AIAA/CEAS Aeroacoustics Conference (28th AIAA Aeroacoustics Conference)*, 2007, pp. 1–20. https://doi.org/10.2514/6.2007-3548.

[13] Scofano, A., Murray, P., and Ferrante, P., "Back-Calculation of Liner Impedance Using Duct Insertion Loss Measurements and FEM Predictions," *13th AIAA/CEAS Aeroacoustics Conference (28th AIAA Aeroacoustics Conference)*, 2007, pp. 1–17. https://doi.org/10.2514/6.2007-3534.

[14] Eversman, W., "Broadband noise suppression for turbofan inlet applications," *International Journal of Aeroacoustics*, Vol. 15, No. 4-5, 2016, pp. 367–394. https://doi.org/10.1177/1475472X16642131.

[15] McAlpine, A., Astley, R., Hii, V., Baker, N., and Kempton, A., "Acoustic scattering by an axially-segmented turbofan inlet duct liner at supersonic fan speeds," *Journal of Sound and Vibration*, Vol. 294, No. 4, 2006, pp. 780–806. https://doi.org/https://doi.org/10.1016/j.jsv.2005.12.039.

[16] Morfey, C., "Sound transmission and generation in ducts with flow," *Journal of Sound and Vibration*, Vol. 14, 1971, pp. 37–55. https://doi.org/10.1016/0022-460X(71)90506-2.

[17] COMSOL, "Acoustics module user's guide," *Version 5.3a*, 2017.

[18] Murray, P., "Sound absorber," *Patent-US2020/0141357*, 2020, pp. 1–16.

[19] Pool, C. L., Udall, K. F., Stretton, R. G., and Reed, J. M., "Duct wall for a fan of a gas turbine engine," *Patent- US 2010/0284790 A1*, 2010, pp. 1–9.

[20] Murray, P., and Astley, R. J., "Development of a single degree of freedom perforate impedance model under grazing flow and high SPL," *18th AIAA/CEAS Aeroacoustics Conference*, 2012. https://doi.org/10.2514/6.2012-2294.

[21] Murray, P., and Astley, R., "Development of a single degree of freedom perforate impedance model under grazing flow and high SPL," *18th AIAA/CEAS Aeroacoustics Conference (33rd AIAA Aeroacoustics Conference)*, 2012, pp. 1–11.

[22] Motsinger, R., and Kraft, R., "Design and performance of duct acoustic treatment," *Aeroacoustics of Flight Vehicles: Theory and Practice*, Vol. 2, No. 14, 1991, pp. 165–206.

[23] Palani, S., Murray, P., McAlpine, A., and Richter, C., "Optimisation of slanted septum core and multiple folded cavity acoustic liners for aero-engines," *AIAA AVIATION FORUM*, 2021, pp. 1–17. https://doi.org/10.2514/6.2021-2172.

[24] MATLAB, "Optimization Toolbox," *The MathWorks, Natick, MA, USA*, R2018a.

[25] Gabard, G., "A comparison of impedance boundary conditions for flow acoustics," *Journal of Sound and Vibration*, Vol. 332, No. 4, 2013, pp. 714–724. https://doi.org/https://doi.org/10.1016/j.jsv.2012.10.014.